International Journal of Thermal Sciences 49 (2010) 1238–1246

Contents lists available at ScienceDirect

International Journal of Thermal Sciences

journal homepage: www.elsevier.com/locate/ijts

Mixed convection on jet impingement cooling of a constant heat flux horizontal porous layer

A. Sivasamy [a,*], V. Selladurai [b], P. Rajesh Kanna [c]

[a] Department of Mechanical Engineering, Sri Krishna College of Engineering and Technology, Coimbatore, Tamil Nadu 641008, India
[b] Department of Mechanical Engineering, Coimbatore Institute of Technology, Coimbatore, Tamil Nadu, India
[c] Department of Mechanical Engineering, Kalasalingam University, Tamil Nadu, India

ARTICLE INFO

Article history:
Received 29 July 2009
Received in revised form
9 January 2010
Accepted 11 January 2010
Available online 20 February 2010

Keywords:
Porous medium
Mixed convection
Impinging slot-jet
Constant heat flux

ABSTRACT

In the present study, numerical investigation of jet impingement cooling of a constant heat flux horizontal surface immersed in a confined porous channel is performed under mixed convection conditions, and the Darcian and non-Darcian effects are evaluated. The unsteady stream function-vorticity formulation is used to solve the governing equations. The results are presented in the mixed convection regime with wide ranges of the governing parameters: Reynolds number ($1 \le Re \le 1000$), modified Grashof number ($10 \le Gr^* \le 100$), half jet width ($0.1 \le D \le 1.0$), Darcy number ($1 \times 10^{-6} \le Da \le 1 \times 10^{-2}$), and the distance between the jet and the heated portion ($0.1 \le H \le 1.0$). It is found that the average Nusselt number (Nu_{avg}) increases with increase in either modified Grashof number or jet width for high values of Reynolds number. The average Nusselt number also increases with decrease in the distance between the jet and the heated portion. The average Nusselt number decreases with the increase in *Da* for the non-Darcy regime when *Re* is low whereas Nu_{avg} increases when *Re* is high. It is shown that mixed convection mode can cause minimum heat transfer unfavorably due to counteraction of jet flow against buoyancy driven flow. Minimum Nu_{avg} occurs more obviously at higher values of *H*. Hence the design of jet impingement cooling through porous medium should be carefully considered in the mixed convection regimes.

1. Introduction

The jet impingement cooling through horizontal porous layer are important from theoretical as well as application points of view. The buoyancy driven phenomena in porous media has attracted researchers interests due to number of technical applications, such as, fluid flow in geothermal reservoirs, insulation of buildings, separation processes in chemical industries, dispersion of chemical contaminants through water saturated soil, solidification of casting, migration of moisture in grain storage system, crude oil production, solar collectors, electronic components cooling, etc. The heat removal of high power density encountered especially in micro-electronic devices can be done effectively using jet impingement of cold fluid. To enhance the heat transfer, porous heat sinks are used in the printed wire board and porous inserts are used in cooling channel of injection mold. These devices could generate high heat flux which induces buoyancy effect. Hence it is important to understand the flow and thermal characteristics of the jet impingement cooling through porous medium. Comprehensive literature survey concerned with this subject is given by Gebhart et al. [1], Kaviany [2], Nield and Bejan [3], Pop and Ingham [4], Bejan and Kraus [5], Ingham et al. [6]. Bejan et al. [7] and Vafai [8]. The literature shows that the jet impingement through pure (non-porous) fluid has been studied extensively (see, for example Al-Sanea [9], Chou and Hung [10], Seyedein et al. [11], Chiriac and Ortega [12], Chung and Luo [13], Sahoo and Sharif [14] and Sivasamy et al. [15]).

Recently many researchers considered the impinging jet through porous media. Fu and Huang [16] investigated numerically the effects of a laminar jet on the heat transfer performance of three different shape (rectangle, convex and concave) porous blocks mounted on a heated plate. They neglected the buoyancy effects and considered the forced convection mode only. Their results show that the heat transfer is mainly affected by a fluid flowing near the heated region. For a lower porous block, all the three type of porous blocks enhance the heat transfer. However, for a higher porous block, the concave porous block only enhances heat transfer. A detailed flow visualization experiment was carried out by Prakash et al. [17] to investigate the effect of a porous layer on flow patterns in an overlying turbulent flow without heat transfer. They studied the effect of the parameters such as the jet Reynolds number, the permeability of the porous foam, the thickness of the

* Corresponding author.
E-mail addresses: a.sivasamy@gmail.com, a_sivasamy@yahoo.com (A. Sivasamy).

1290-0729/$ – see front matter © 2010 Elsevier Masson SAS. All rights reserved.
doi:10.1016/j.ijthermalsci.2010.01.010

porous foam and the height of the overlying fluid layer. Jeng and Tzeng [18] studied numerically the air jet impingement cooling of a porous metallic foam heat sink in the forced convection mode. They found the porous aluminum foam heat sink could enhance the heat transfer from the heated horizontal source by impinging cooling. Their results show that the heat transfer performance of the aluminum foam heat sink is 2–3 times larger than that without it. Saeid and Mohamad [19] studied numerically the jet impingement cooling of heated portion of an isothermal horizontal surface immersed in a fluid saturated porous media in the mixed convection regime. It was found for high values of Peclet number at increasing either Rayleigh number or jet width lead to increase the average Nusselt number. Narrowing the distance between the jet and the heated portion could increase the average Nusselt number. Recently Jeng et al. [20] carried out experimental investigation on heat transfer associated with air jet impingement on rotating porous Aluminum foam heats sink. They investigated the effects of jet Reynolds number (Re) in the forced convection mode, the relative nozzle-to-foam tip distance (C/d), the rotational Reynolds number (Re_r) and the relative side length of the square heat sink (L/d). They found that, when Re and L/d were small and C/d was large, the increase in Re_r increases the average Nusselt number.

Tong and Subramanian [21], Lauriat and Prasad [22], and Prasad et al. [23] demonstrated the Brinkman-extended Darcy flow model in the numerical investigation on natural convection in a vertical porous layer. They highlighted the importance of Brinkman equation in convection of porous media. Hadim and Chen [24] reported a numerical study of buoyancy-aided mixed convection in an isothermally heated vertical channel filled with a fluid saturated porous medium using the Darcy–Brinkman–Forchheimer model. Their results show that, the effect of decreasing Darcy number is, however, important only at low values of Darcy number (in the Darcy Regime). At large Darcy number, the flow in this region is dominated by forced convection and the Nusselt number is almost independent of Da. Wong and Saeid [25] numerically investigated the jet impingement cooling of heated portion of an isothermal horizontal surface immersed in a confined porous channel under mixed convection conditions with Brinkman-extended Darcy model. The results were presented in the mixed convection regime with wide ranges of Rayleigh number (Ra), Péclet number (Pe), jet width and Darcy number (Da) in Darcy regime and non-Darcy regime. The average Nusselt number decreases with the increase in Da for the non-Darcy regime when Pe is low. When Pe is high, the average Nusselt number increases with the increase in Da for the non-Darcy regime. Variation of Da in Darcy regime has negligible effect on the heat transfer performance.

In many application the hot surface may be at constant heat flux instead of being isothermal, for example, embedded electronic component on a circuit board. Whenever there is a large temperature difference between the working fluid and the horizontal heated surface with constant heat flux source and the flow velocity is not significantly high, there might be some effect of thermal buoyancy force. It is important to understand the effects of buoyancy in the heat transfer and flow characteristics for designing the cooling system when impinging jet cooling process operates in mixed convection regime. This is the main motivation for this study. It is interesting to investigate the effect of the Darcy number for the jet impingement cooling of a constant heat flux horizontal channel with fluid saturated porous medium.

2. Problem description

In the present study, the effect of the buoyancy on the jet impingement cooling of a constant heat flux horizontal surface immersed in a fluid saturated porous media is considered as shown in Fig. 1. The objective of the present study is to characterize the thermal performance of the jet impingement cooling in porous media in the mixed convection regime.

The governing parameters in the present problem are the half jet width d, the jet velocity V_0, the distance between the jet and the heated portion h, and the heat source length $2L$ in additional to the physical properties of the porous media and the fluid. These parameters can be reduced to a number of dimensionless groups as given in the next section. The physical properties are assumed to be constant except the density in the buoyancy force term which is satisfied by the Boussinesq's approximation. Further it is assumed that the temperature of the fluid phase is equal to the temperature of the solid phase everywhere in the porous region, and local thermal equilibrium (LTE) model is applicable in the present investigation.

Under these assumptions, the conservation equations for mass, momentum and energy for the two-dimensional unsteady flow can be written as: [25]

$$\frac{\partial u}{\partial x}+\frac{\partial v}{\partial y}=0 \tag{1}$$

$$\rho\frac{\partial u}{\partial t^*}+\rho u\frac{\partial u}{\partial x}+\rho v\frac{\partial u}{\partial y}=-\frac{\partial P}{\partial x}+\mu\left(\frac{\partial^2 u}{\partial x^2}+\frac{\partial^2 u}{\partial y^2}\right)-\frac{\mu}{K}u \tag{2}$$

$$\rho\frac{\partial v}{\partial t^*}+\rho u\frac{\partial v}{\partial x}+\rho v\frac{\partial v}{\partial y}=-\frac{\partial P}{\partial y}+\mu\left(\frac{\partial^2 v}{\partial x^2}+\frac{\partial^2 v}{\partial y^2}\right)-\frac{\mu}{K}v+\rho\beta g(T-T_\infty) \tag{3}$$

$$\frac{\partial T}{\partial t^*}+u\frac{\partial T}{\partial x}+v\frac{\partial T}{\partial y}=\alpha\left(\frac{\partial^2 T}{\partial x^2}+\frac{\partial^2 T}{\partial y^2}\right) \tag{4}$$

The following dimensionless parameters are adopted in the present study:

$$t=\frac{t^* V_0}{L}\quad X=\frac{x}{L}\quad Y=\frac{y}{L}\quad U=\frac{u}{V_0}=\frac{\partial \Psi}{\partial Y}\quad V=\frac{v}{V_0}=-\frac{\partial \Psi}{\partial X}$$
$$\theta=\frac{T-T_c}{\Delta T}\quad \Delta T=\frac{q''L}{k}$$

From Equations (1)–(4), the following non-dimensionless equations are obtained:

$$\frac{\partial^2 \Psi}{\partial X^2}+\frac{\partial^2 \Psi}{\partial Y^2}=-\omega \tag{5}$$

$$\frac{\partial \omega}{\partial t}+U\frac{\partial \omega}{\partial X}+V\frac{\partial \omega}{\partial Y}=\frac{1}{Re}\left(\frac{\partial^2 \omega}{\partial X^2}+\frac{\partial^2 \omega}{\partial Y^2}\right)-\frac{1}{ReDa}\omega+\frac{Gr^*}{\mathrm{Re}^2 Da}\frac{\partial \theta}{\partial X} \tag{6}$$

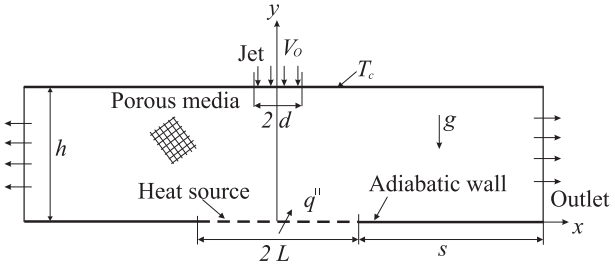

Fig. 1. Schematic diagram of the physical model and coordinate system.

$$\frac{\partial\theta}{\partial t}+U\frac{\partial\theta}{\partial X}+V\frac{\partial\theta}{\partial Y}=\frac{1}{RePr}\left(\frac{\partial^2\theta}{\partial X^2}+\frac{\partial^2\theta}{\partial Y^2}\right) \tag{7}$$

where the vorticity, modified Grashof number, Reynolds number, Darcy number and Prandtl number are defined respectively as

$$\omega=\frac{\partial V}{\partial X}-\frac{\partial U}{\partial Y}\quad Gr^*=\frac{g\beta K\Delta TL}{\nu^2}\quad Re=\frac{V_0L}{\nu}\quad Da=\frac{K}{L^2}\quad Pr=\frac{\nu}{\alpha}$$

The flow and heat transfer characteristics are symmetrical around y-axis as shown in Fig. 1. Due to this symmetry, only one half is considered for the computational purpose and the boundary conditions are

At $X=0$ (Symmetrical axis):

$$U(0,Y)=\frac{\partial V(0,Y)}{\partial X}=\frac{\partial\Psi(0,Y)}{\partial X}=\frac{\partial\omega(0,Y)}{\partial X}=\frac{\partial\theta(0,Y)}{\partial X}=0$$

At $X=1+S$ (flow exit):

$$\frac{\partial U(1+S,Y)}{\partial X}=\frac{\partial V(1+S,Y)}{\partial X}=\frac{\partial^2\Psi(1+S,Y)}{\partial X^2}=0$$

$$\frac{\partial\omega(1+S,Y)}{\partial X}=\frac{\partial\theta(1+S,Y)}{\partial X}=0$$

At $Y=0$ (lower surface):

$$U(X,0)=V(X,0)=\Psi(X,0)=0\quad\omega(X,0)=-\frac{\partial^2\psi}{\partial Y^2}$$

$$\frac{\partial\theta(X,0)}{\partial Y}=\begin{cases}-1 & \text{if } 0\le X\le L\\ 0 & \text{if } X>L\end{cases}$$

At $Y=1$ (upper surface):

$$\omega(X,1)=-\frac{\partial^2\psi}{\partial Y^2}\quad U(X,1)=\theta(X,1)=0$$

$$\Psi(X,1)=\begin{cases}X & \text{if } 0\le X\le D\\ D & \text{if } X>D\end{cases}\quad V(X,1)=\begin{cases}-1 & \text{if } 0\le X\le D\\ 0 & \text{if } X>D\end{cases}$$

The physical quantities of interest in the present investigation are the local and the average Nusselt numbers along the heat source which are defined respectively as

$$Nu(X)=-\frac{1}{\theta}\Big|_{Y=0}\quad Nu_{avg}=\frac{1}{L}\int_0^L Nu(X)dX \tag{8}$$

3. Numerical procedure

The convective, the diffusive and the buoyancy terms in the governing equations are discretized with a central difference formulation. The unsteady vorticity transport equation (6) and energy equation (7) in time are solved by alternate direction implicit (ADI) scheme. The stream function equation (5) is solved by the successive over relaxation (SOR) method. Roache [26] gives a thorough discussion of the ADI and SOR schemes. The present code is a modified version of code developed in [27].

Table 1
Grid refinement scheme: $H=1.0$, $Gr^*=100$, $Re=100$, and $Da=10^{-6}$.

Grid refinement level	Y direction	X direction		Nu_{avg}	
		$0\le X\le L$	$X>L$	$D=0.1$	$D=1.0$
Grid 1	11	10	21	2.9132	7.0180
Grid 2	21	20	31	2.8379	6.6183
Grid 3	31	30	41	2.8122	6.5055
Grid 4	41	40	51	2.7987	6.4620

Table 2
The comparison of average Nusselt number (Nu_{avg}) values with Wong and Saeid [25] for $H=1.0$, $D=0.1$, $Ra=100$, and $Da=10^{-6}$ and Saeid et al. [19] (Darcy model).

$Pe=RePr$	Wong and Saeid [25]	Saeid et al. [19]	This study
1	4.011	3.894	3.8741
10	4.140	4.017	4.0528
40	3.095	3.141	3.0811
100	3.571	3.627	3.6135
1000	8.778	9.016	8.9291

In X direction up to heat source length (L) the grids are arranged uniformly after that clustered. In Y direction grids are clustered near top and bottom walls. A systematic grid refinement study is conducted to obtain grid independent solutions. The grid refinement scheme is shown in Table 1. The computations are performed for $H=1$, $D=0.1, 1.0$, $Gr^*=100$, $Re=100$, and $Da=10^{-6}$ for various grid refinement levels as shown in the Table 1. It is observed that grid refinement level 3 produced almost grid independent results and thus grid refinement level 3 is used for the entire computations.

The validation of the results against the numerical results of the study by Wong and Saeid [25], whose geometry and flow parameters are quite similar to the present study are reproduced using the present code. Wong and Saeid [25] used a different computational procedure (Finite volume method with power law scheme). The average Nusselt number at the heat source predicted by the present computer code is compared with Wong and Saeid [25] for various Péclet number with $H=1.0$, $D=0.1$, $Ra=100$, and $Da=10^{-6}$ in Table 2. The agreement is found to be good. The results of present study in the Darcy regime matched well with Darcy model used by Saeid et al.[19].

4. Results and discussion

The results are presented as average Nusselt number against Reynolds number for different values of the parameters Gr^*, D, Da and H. The range of the parameters are $1\le Re\le 1000$, $10\le Gr^*\le 100$, $0.1\le D\le 1.0$, $1\times10^{-6}\le Da\le 1\times10^{-2}$ and $0.1\le H\le 1.0$. The Prandtl number for air ($Pr=0.71$) is fixed throughout the study.

The variation of average Nusselt number against Reynolds number for different values of modified Grashof number is shown

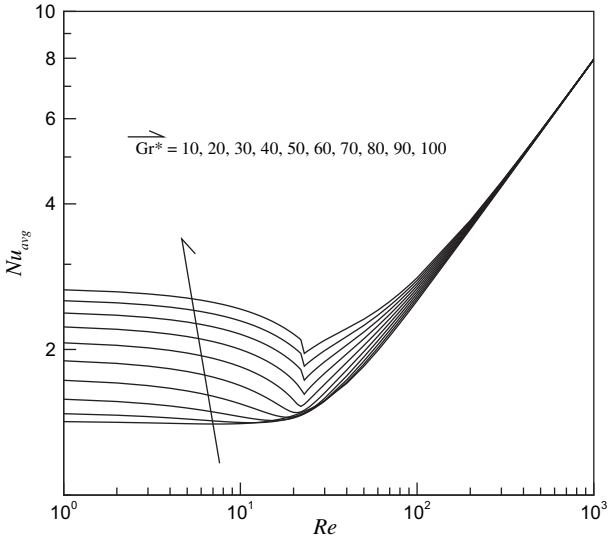

Fig. 2. Variation of average Nusselt number with Peclet number with $H=1$, $D=0.1$ and $Da=10^{-6}$.

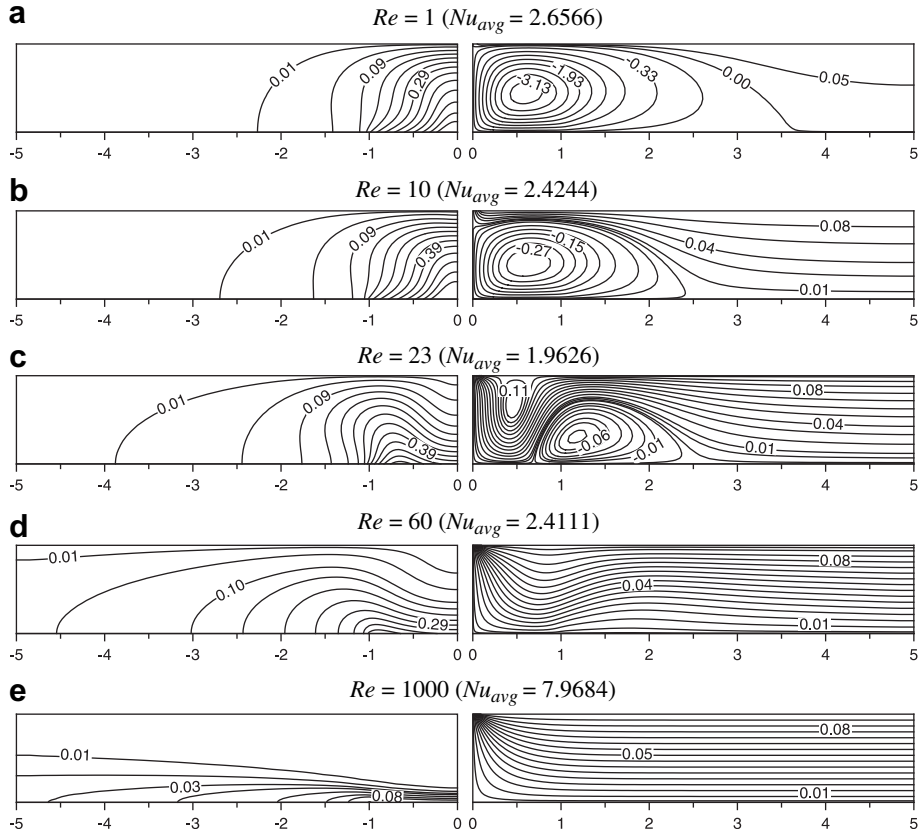

Fig. 3. Isotherms (left), streamlines (right) with $H = 1.0$, $D = 0.1$, $Gr^* = 100$, and $Da = 10^{-6}$.

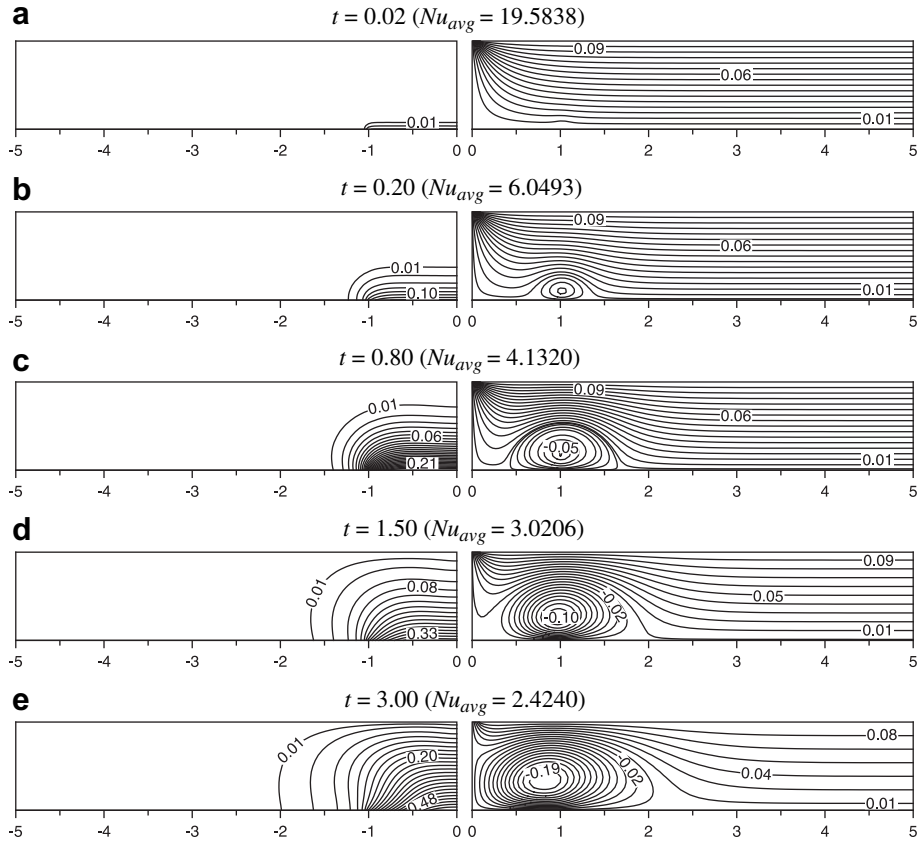

Fig. 4. Isotherms (left), streamlines (right) with $H = 1.0$, $D = 0.1$, $Re = 10$, and $Ra = 100$.

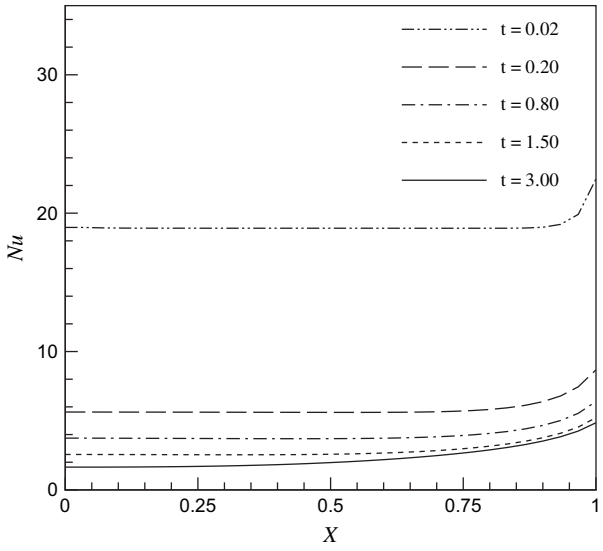

Fig. 5. Variation of local Nusselt number with time (t) for $H = 1.0$, $D = 0.1$, $Re = 10$, and $Gr^* = 100$.

in Fig. 2 with fixed values of $H = 1$, $D = 0.1$ and $Da = 10^{-6}$. Note that in Fig. 2, the logarithmic scale is used for both Nu_{avg} and Re.

In the cases of natural convection domination at low values of Reynolds number, the increase in the Reynolds number decreases the average Nusselt number for $Gr^* > 10$ and the change of Re gives negligible changes on the heat transfer at $Gr^* = 10$. However, the increase in the modified Grashof number increases the average Nusselt number as shown in Fig. 2. At forced convection domination with high values of Re, Fig. 2 shows that the effect of modified Grashof number is diminished and the variation of Nu_{avg} with Re for different values of Gr^* forming a single curve for $Re > 300$. It can be observed from Fig. 2 that the values of Nu_{avg} and therefore the heat transfer show minimum values for moderate values of Reynolds number with $Gr^* > 10$. These values of Re which result in minimizing the heat transfer are in-between the values of Re for natural and forced convection domination, which is known as mixed convection. The present mixed convection mode is of opposing nature since the jet flow is always opposing the buoyant flow. The value of Re at which minimum Nu_{avg} occurs depends on Gr^*.

Fig. 3 shows the details of isotherms and streamlines for different values of Re with fixed values of $H = 1.0$, $D = 0.1$, $Gr^* = 100$, and $Da = 10^{-6}$, as to interpret graphically the mixed convection mode discussed on Fig. 2. The isotherms and streamlines shown in Fig. 3(a) and (b) for $Re = 1$ and $Re = 10$ respectively indicating natural convection domination. The isotherms are cluster above the heat source and one convective vortex rotating opposite to jet fluid direction is formed above the heat source (Fig. 3(a)). At $Re = 10$, jet fluid depresses the rise of the single vortex rotating the fluid formed above the heat source (Fig. 3(b)). It is also noticed that the strength of the cell is reduced and the vortex becomes weaker, leading to reduction of Nu_{avg}.

It is interesting to see the transient responses of the flow and temperature fields at this Re (Fig. 4). The time step 0.001 is used for the computation. The figure denotes that the initial action of the impinging jet that enters in the saturated porous layer is similar to that of the free jet (Fig. 4(a)). Sudden heating at $t > 0$ at the bottom horizontal heat source creates sharp temperature gradients in the proximity of the horizontal heat source. At this moment heat transfer is high due to the sharp temperature

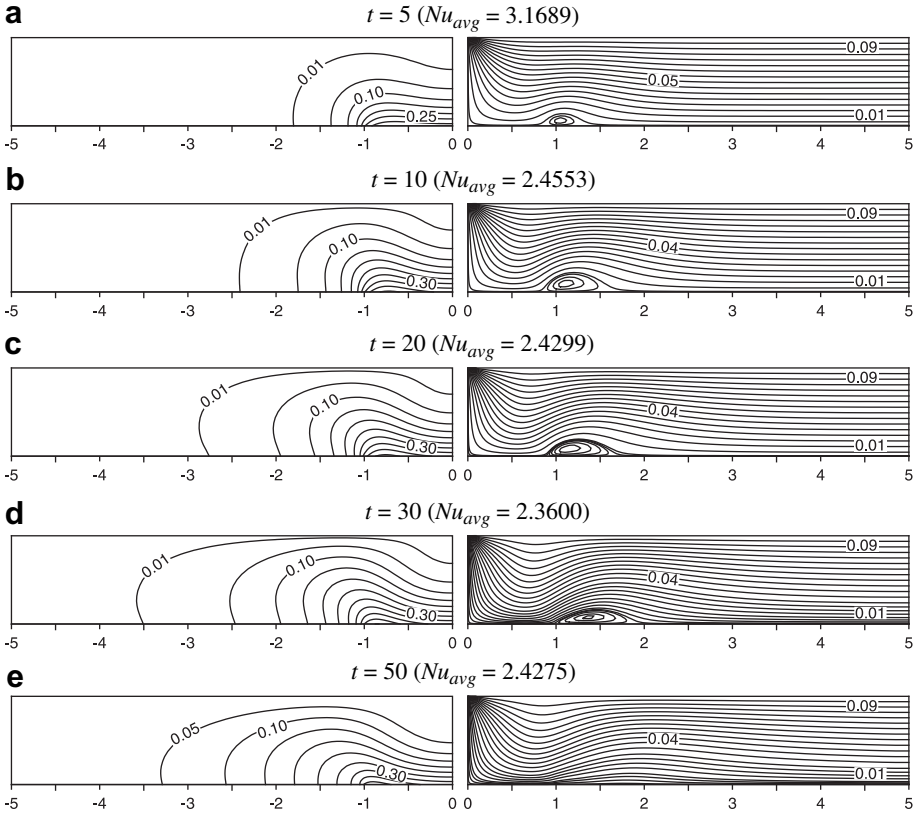

Fig. 6. Isotherms (left), streamlines (right) with $H = 1.0$, $D = 0.1$, $Re = 60$, and $Gr^* = 100$.

gradients. A small vortex is formed at the end of the heat source ($X = 1.0$) at $t = 0.20$ (Fig. 4(b)). This vortex grows as time increases and the center of the vortex is located at the end of the heat source (Fig. 4(b–c)). It can be seen from Fig. 4(d) that the jet fluid reaches the bottom heat source and prevents the movement of the vortex upstream direction. It is noticed from Fig. 4(e) that the vortex grows and becomes stronger as time increases further. The vortex moves upstream direction and stops the weak jet fluid reaching the bottom heat source. As time increases the temperature gradients decrease in the horizontal heat source and cause the reduction in the average Nusselt number and hence heat transfer. It can be seen from Fig. 5 that the local Nusselt number decreases along the heat source as time increases. The Nu is maximum at the end of the heat source ($X = 1.0$) due to the formation of convective vortex. The flow achieves its steady state at large t (Fig. 3(b)).

At $Re = 23$, Fig. 2 shows that $Nu_{avg} = 1.9626$ which is the minimum value for $Gr^* = 100$, the isotherms and streamlines for this case are shown in Fig. 3(c). At this value of Re, the jet flow prevents the growth of the bottom convective vortex by the buoyant flow (as seen in transient results at $Re = 10$) towards the jet axis and pushes it downstream. The strength of the vortex is also less. Another vortex rotating the jet fluid direction (comparatively stronger than bottom vortex) is formed near the jet inlet. The isotherms are modified as well, where the isotherms are compressed against the heat source from jet axis to a point where the jet flow separates from the horizontal heat source.

In the forced convection domination, where Re is high, the two rotating vortices disappear (explained below with transient results) as shown in Fig. 3(d) and (e). The isotherms show high negative gradients; especially in Fig. 3(e), which leads to increase the heat transfer from the heat source. Fig. 6 presents numerically simulated isotherms and streamlines plot at various time levels for $H = 1$, $D = 0.1$, $Re = 60$ and $Gr^* = 100$. A small vortex is formed at the end of the heat source at $t = 5$ (Fig. 6(a)). This vortex grows as time increases and the center of the vortex moves downstream as the jet flow is stronger (Fig. 6(b–c)). Fig. 6(d) shows that the strong jet flow pushes away the vortex. The size of the vortex becomes small as t increases and vanishes at $t = 50$ (Fig. 6(e)). As time increases the temperature gradients decrease in the horizontal heat source and cause the reduction in the average Nusselt number and hence heat transfer. Fig. 7 shows the distribution of local Nusselt number along the heat source with time (t). At $t \leq 20$, Nu is maximum at the end of heat source due to the convective vortex. However Nu is minimum at the end of heat source as vortex moves away and vanishes at $t \geq 30$. The steady state solution is shown in Fig. 3(d).

The effect of the distance from the jet exit to the heat source (H) on the variation of Nu_{avg} with Re is studied with constant values of other parameters ($D = 0.5$, $Gr^* = 50$, and $Da = 10^{-6}$). For natural convection domination ($Re < 4$), Fig. 8 shows that Nu_{avg} decreases with the increase in Re for $H \geq 0.8$ where as Nu_{avg} is constant with increase in Re for $H < 0.8$. Minimum Nu_{avg} occurs more obviously at higher values of H. It can be noticed from Fig. 8 that the values of Nu_{avg} are increasing with the increase of Re in the forced convection domination mode, similar to that shown in Fig. 2. The variation of Nu_{avg} with Re is linear, when the logarithmic scale is used as shown in Fig. 8. The heat transfer rate is increased when the distance from the jet exit to the heat source (H) is reduced. Fig. 8 also shows that narrowing the distance H from 0.2 to 0.1 leads to substantial increase in Nu_{avg}. While the enhancement of the heat transfer due to the change of H from 1 to 0.5 is relatively less than that due to narrowing the distance H from 0.2 to 0.1 especially at low values of Re.

Fig. 9 shows the details of isotherms and streamlines for different values of H with fixed values of $Re = 1.0$, $D = 0.5$, $Gr^* = 50$, and $Da = 10^{-6}$, as to interpret graphically the effect of the distance

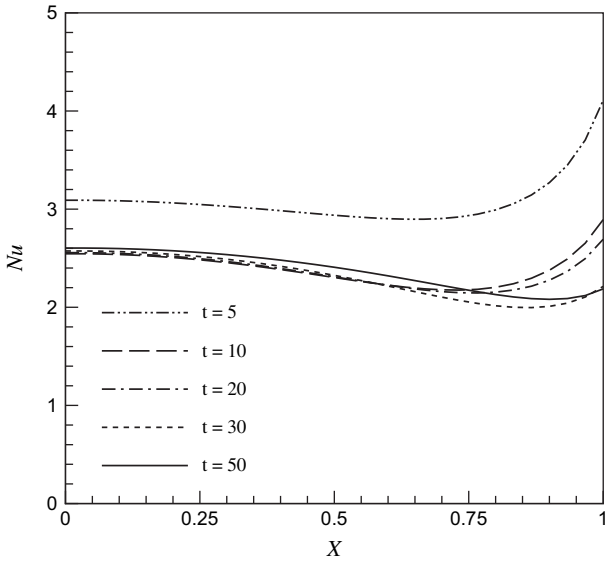

Fig. 7. Variation of local Nusselt number with time (t) for $H = 1.0$, $D = 0.1$, $Re = 60$, and $Gr^* = 100$.

from the jet exit to the heat source discussed on Fig. 8. At $H = 1.0$, the single convective vortex occupies the entire space above the heat source and the jet flow is unable to reach the bottom heat source due to strong buoyant flow (Fig. 9(a)). As H decreases the size and the strength of the vortex decrease due to decrease in the buoyant flow. Hence the convective vortex is unable to move upstream against the jet fluid flow and jet flow reaches the bottom heat source (Fig. 9(c–e)). At very low H ($H \leq 0.2$) the convective vortex vanishes (Fig. 9(e)). The isotherms become parallel to horizontal heat source surface as H decreases (Fig. 9 (c–e)). This is the indication of forced convection domination which causes the increase in heat transfer. The buoyant flow decreases rapidly as H decreases and hence Nu_{avg} increases much at low H as noticed in Fig. 8.

Next, the variation of the average Nusselt number with Reynolds number is presented in Fig. 10 with different values of the half jet

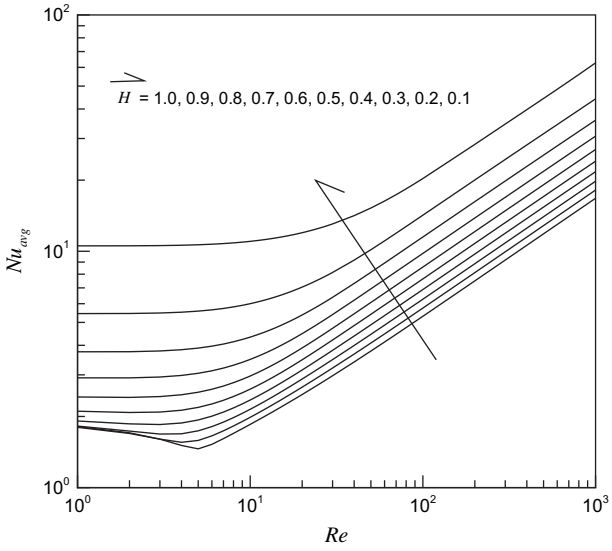

Fig. 8. Variation of average Nusselt number with Péclet number with $D = 0.5$, $Gr^* = 50$, and $Da = 10^{-6}$.

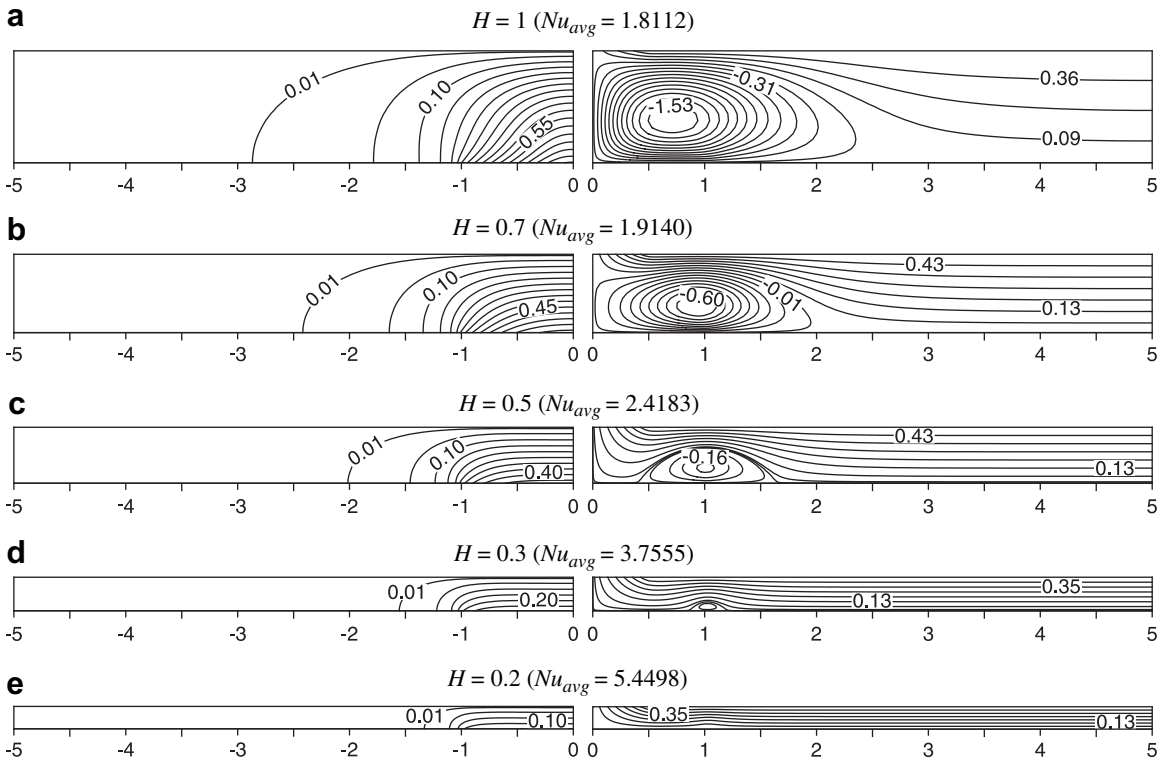

Fig. 9. Isotherms (left), streamlines (right) with $Re = 1.0$, $D = 0.5$, $Gr^* = 50$, and $Da = 10^{-6}$.

width D and fixed values of $H = 1$, $Gr^* = 50$ and $Da = 10^{-4}$. Fig. 10 shows that at small values of Re, where the natural convection dominated the average Nusselt number with small jet width is more than that of big jet width. This is due to the fact that small jet width D generating weak opposing flow to the buoyant flow for this limits of Re and Gr^*. The average Nusselt number with high values of D is higher than that at small values of D in the forced convection domination mode. This indicates the effect of increasing the jet mass flow rate by increasing D and hence increasing the forced convective heat transfer. The values of Nu_{avg} show minimum values for moderate values of Reynolds number in the considered range of D. The value of Re at which minimum Nu_{avg} occurs depends on D. As D increases the value of Re at which minimum Nu_{avg} occurs decreases.

Fig. 11 depicts the variation of average Nusselt number against Reynolds number for different values of Da with fixed values of $D = 0.1$ and $Gr^* = 100$. It can be seen in Fig. 11 that, the variation of Nu_{avg} at any particular Re is approximately constant regardless

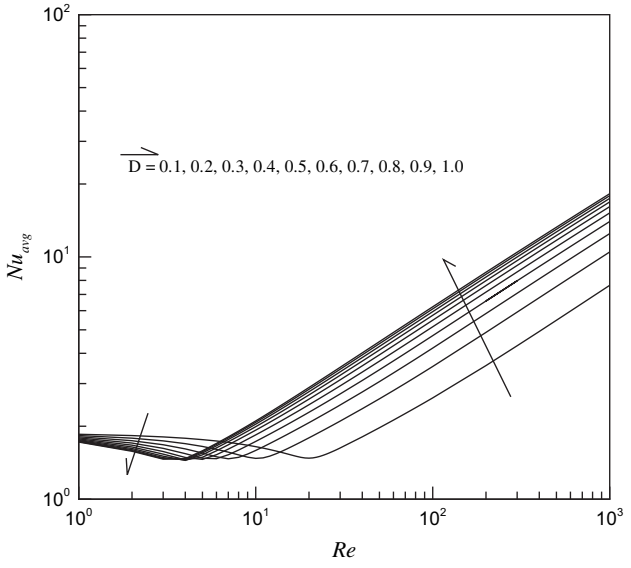

Fig. 10. Variation of average Nusselt number with Reynolds number for $H = 1$, $Gr^* = 50$ and $Da = 10^{-4}$.

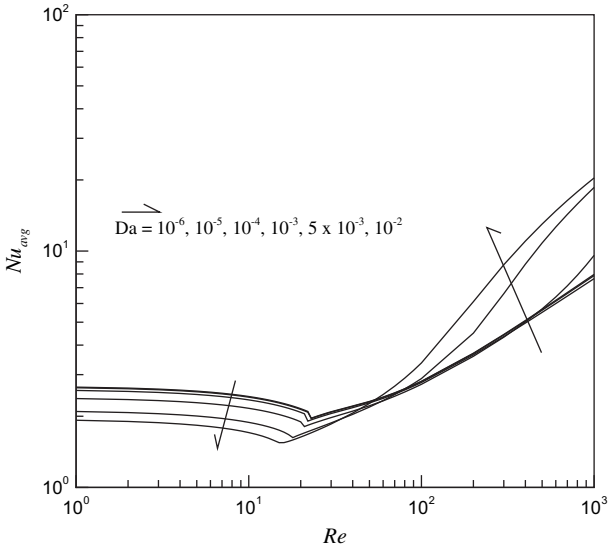

Fig. 11. Variation of average Nusselt number with Reynolds number for $H = 1$, $Gr^* = 100$ and $D = 0.1$.

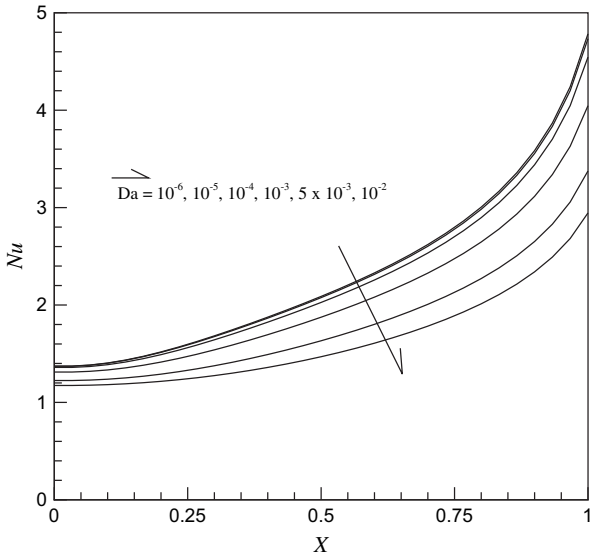

Fig. 12. Variation of local Nusselt number for different Darcy number, with fixed $Re = 10$, $D = 0.1$ and $Gr^* = 100$.

of the value of Darcy number for $Da < 10^{-4}$. The regime of low Darcy value ($Da < 10^{-4}$) is known as Darcy regime and the regime for $Da \leq 10^{-4}$ is known as non-Darcy regime [24]. Variation of Da in Darcy regime has negligible effect on the heat transfer performance. Fig. 11 also shows that, the average Nusselt number decreases with the increase in Darcy number for the non-Darcy regime when Re is low ($Re < 23$). This agrees with the results obtained by Hadim and Chen [24] that, at low value of Reynolds number, as Darcy number increases, the heat transfer performance reduces. When Re is high, the average Nusselt number increases with the increase in Darcy number for the non-Darcy regime. Fig. 12 presents the local Nusselt numbers for different values of Darcy number with fixed values of $Re = 10$, $D = 0.1$ and $Gr^* = 100$. For each curve in Fig. 12, the heat transfer along X shows minimum local Nusselt number at the jet axis and higher local Nusselt number at the end of heat source ($X = 1.0$). The local Nusselt number along the heat source decreases with increase of Da in the non-Darcy regime.

5. Conclusions

The jet impingement cooling of a constant heat flux horizontal surface immersed in a fluid saturated porous media is investigated numerically. The external jet flow and the buoyancy driven flow are chosen to be in opposite direction. The dimensionless governing parameters results from the mathematical model are the Darcy number, modified Grashof number, Reynolds number, jet width and the distance between the jet and the heated portion normalized to the length of the heated element. After validation of the numerical method, the results are presented in the mixed convection regime with wide ranges of the governing parameters. The specific conclusions obtained from the present study can be summarized as follows:

- The low values of Reynolds number at increasing the modified Grashof number increases the average Nusselt number, and the increase become less significant when Reynolds number increase to high value.
- Increase in the value of jet width results in higher average Nusselt number for high values of Reynolds number.
- The heat transfer rate is increased when the distance from the jet exit to the heat source is reduced.
- The value of Re at which minimum Nu_{avg} occurs depends on Gr^*, D and H. As D increases the value of Re at which minimum Nu_{avg} occurs decreases. Minimum Nu_{avg} occurs more obviously at higher values of H.
- The average Nusselt number decreases with the increase in Darcy number for the non-Darcy regime when Re is low ($Re < 23$). When Re is high, the average Nusselt number increases with the increase in Darcy number for the non-Darcy regime. Variation of Da in Darcy regime has negligible effect on the heat transfer performance.

Acknowledgements

The constructive comments and suggestions of the reviewers are sincerely acknowledged by the authors.

References

[1] B. Gebhart, Y. Jaluria, R.L. Mahajan, B. Sammakia, Buoyancy-induced Flows and Transport. Hemisphere, New York, 1988.
[2] M. Kaviany, Principles of Heat Transfer in Porous Media, second ed. Springer-Verlag, New York, 1995.
[3] D.A. Nield, A. Bejan, Convection in Porous Media, third ed. Springer-Verlag, New York, 2006.
[4] I. Pop, D.B. Ingham, Convective Heat Transfer: Mathematical and Computational Modelling of Viscous Fluids and Porous Media. Pergamon, Oxford, 2001.
[5] A. Bejan, A.D. Kraus (Eds.), Heat Transfer Handbook, Wiley, New York, 2003.
[6] D.B. Ingham, A. Bejan, E. Mamut, I. Pop (Eds.), Emerging Technologies and Techniques in Porous Media, Kluwer, Dordrecht, 2004.
[7] A. Bejan, I. Dincer, S. Lorente, A.F. Miguel, A.H. Reis, Porous and Complex Flow Structures in Modern Technologies. Springer, New York, 2004.
[8] K. Vafai, Handbook of Porous Media, second ed. Marcel Dekker, New York, 2005.
[9] S. Al-Sanea, A numerical study of the flow and heat transfer characteristics of an impinging laminar slot-jet including crossflow efffects. International Journal of Heat and Mass Transfer 35 (1992) 2501–2513.
[10] Y.J. Chou, Y.H. Hung, Impingement cooling of an isothermally heated surface with a confined slot jet. Journal Heat Transfer 116 (1994) 2137–2145.
[11] S.H. Seyedein, M. Hasan, A.S. Mujumdar, Laminar flow and heat transfer from multiple impinging slot jets with an inclined confinement surface. International Journal of Heat and Mass Transfer 37 (1994) 1867–1875.
[12] V.A. Chiriac, A. Ortega, A numerical study of the unsteady flow and heat transfer in a transitional confined slot jet impinging on an isothermal surface. International Journal of Heat and Mass Transfer 45 (2002) 1237–1248.
[13] Y.M. Chung, K.H. Luo, Unsteady heat transfer analysis of a impinging jet. Journal of Heat Transfer 124 (2002) 1039–1048.
[14] D. Sahoo, M.A.R. Sharif, Numerical modeling of slot-jet impingement cooling of a constant heat flux surface confined by a parallel wall. International Journal of Thermal Sciences 43 (2004) 877–887.
[15] A. Sivasamy, V. Selladurai, P.R. Kanna, Numerical simulation of two-dimensional laminar slot-jet impingement flows confined by a parallel wall. International Journal for Numerical Methods in Fluids 55 (2007) 965–983.
[16] W.S. Fu, H.C. Huang, Thermal performance of different shape porous blocks under an impinging jet. International Journal of Heat and Mass Transfer 40 (1997) 2261–2272.
[17] M. Prakash, O.F. Turan, Y. Li, J. Mahoney, G.R. Thorpe, Impinging round jet studies in a cylindrical enclosure with and without a porous layer: Part I – flow visualizations and simulations. Chemical Engineering Science 56 (2001) 3855–3878.
[18] T.M. Jeng, S.C. Tzeng, Numerical study of confined slot jet impinging on porous metallic foam heat sink. International Journal of Heat and Mass Transfer 48 (2005) 4685–4694.
[19] N.H. Saeid, A.A. Mohamad, Jet impingement cooling of a horizontal surface in a confined porous medium: mixed convection regime. International Journal of Heat and Mass Transfer 49 (2006) 3906–3913.
[20] T.M. Jeng, S.C. Tzeng, T.C. Liu, Heat transfer behavior in a rotating aluminum foam heat sink with a circular impinging jet. International Journal of Heat and Mass Transfer 51 (2008) 1205–1215.
[21] T.W. Tong, E. Subramanian, A boundary-layer analysis for natural convection in vertical porous enclosures—use of the brinkman-extended darcy model. International Journal of Heat and Mass Transfer 28 (1985) 563–571.
[22] G. Lauriat, V. Prasad, Natural convection in a vertical porous cavity: a numerical study for brinkman-extended darcy formulation. Journal of Heat Transfer 109 (1987) 688–696.
[23] V. Prasad, G. Lauriat, N. Kladias, Re-examination of Darcy–Brinkman solutions for free convection in porous media, in: ASME Proceedings of the 1988 National Heat Transfer Conference, vol. 1, 1988, pp. 569–580.

[24] H.A. Hadim, G. Chen, Numerical study of non-darcy mixed convection in a vertical porous channel. J. Thermophys 8 (1993) 371–373.
[25] K.C. Wong, N.H. Saeid, Numerical study of mixed convection on jet impingement cooling in a horizontal porous layer-using brinkman-extended darcy model. International Journal of Thermal Sciences 48 (2009) 96–104.
[26] P.J. Roache, Computational Fluid Dynamics, rev. ed., Hermosa, Albuquerque, New Mexico, 1982.
[27] P. Rajesh Kanna, Flow and conjugate heat transfer study of wall bounded laminar plane jet flows, Ph.D. thesis, Indian Institute of Technology Guwahati, 2005.

Nomenclature

d: half of the width of the jet (m)
D: half of the dimensionless width of the jet, $D = d/L$
Da: Darcy number, $Da = K/L^2$
g: acceleration due to gravity (ms^{-2})
Gr^*: modified Grashof number for porous medium, $Gr^* = g\beta K\Delta TL/\nu^2$
h: distance between the jet and the heated portion (m)
H: dimensionless distance between the jet and the heated portion
k: thermal conductivity ($Wm^{-1}\,K^{-1}$)
K: permeability of the porous medium (m^2)
L: half of the heat source length (m)
Nu: local Nusselt number
p: pressure (Pa)
Pe: Péclet number, $Pe = V_0L/\alpha$
Ra: Rayleigh number for porous medium, $Ra = g\beta K\Delta TL/\nu\alpha$
Re: Reynolds number, $Re = V_0L/\nu$
q'': heat flux per unit area (Wm^{-2})
s: distances from the end of heated portion to the outlet, (m)
S: dimensionless distances from the end of heated portion to the outlet, s/L
t: non-dimensional time
t^*: time (s)
T: temperature (K)
u, v: velocity components along x- and y-axes, respectively (ms^{-1})
V_0: jet velocity (ms^{-1})
U, V: non-dimensional velocity components along X and Y-axes, respectively
x, y: Cartesian coordinates (m)
X, Y: non-dimensional Cartesian coordinates

Greek symbols

α: effective thermal diffusivity (m^2s^{-1})
β: coefficient of thermal expansion (K^{-1})
θ: non-dimensional temperature
μ: dynamic viscosity (Nsm^{-2})
ν: kinematic viscosity (m^2s^{-1})
ρ: density (kgm^{-3})
Ψ: non-dimensional stream function
ω: non-dimensional vorticity

Subscripts

avg: average